A computer model of a cochlear-nucleus stellate cell: Responses to amplitude-modulated and pure-tone stimuli

Michael J. Hewitt, Ray Meddis, and Trevor M. Shackleton
Speech and Hearing Laboratory, Department of Human Sciences, University of Technology, Loughborough LE11 3TU, United Kingdom

(Received 13 August 1991; accepted for publication 13 December 1991)

A computer model of a ventral-cochlear-nucleus (VCN) stellate cell with chop-S type response properties is presented and evaluated. The model is based on a simplified model of spike generation preceded by a stage that simulates dendritic low-pass filtering. Input to the model is in the form of simulated auditory-nerve spikes produced by a model of the auditory periphery [Meddis and Hewitt, J. Acoust. Soc. Am. **89**, 2866–2882 (1991)]. Outputs from the stellate-cell model are shown to qualitatively replicate a wide range of typical *in vivo* responses. These include: (a) realistic onset and steady-state rate-level functions, (b) "chopper"-type post-stimulus time histogram responses; (c) typical "chop-S"-type neuron responses characterized by a low coefficient of variance (CV < 0.3) of interspike intervals as a function of time; (d) level-dependent amplitude-modulation transfer functions; (e) intrinsic oscillations in responses to pure-tone stimuli; (f) amplitude-modulation encoding over a wide dynamic range; and (g) frequency-limited phase locking to pure tones. It is shown that these responses can be explained primarily by the membrane properties of the cells. More specifically, how the model encodes signal amplitude modulation was studied and an explanation was suggested for the generation of the bandpass modulation transfer functions. Such functions are observed neurally in response to amplitude-modulated stimuli presented at moderate to high signal levels.

PACS numbers: 43.64.Qh, 43.64.Bt

INTRODUCTION

The first major nucleus of the central auditory pathway is the cochlear nucleus (CN) complex. The complex is divided into three major divisions (anteroventral, posteroventral, and dorsal) on the basis of differing cytoarchitecture (Osen, 1969) and the existence of three separate tonotopic frequency maps (Rose *et al.*, 1960). The three divisions also show broadly different physiological response properties, and it is likely, therefore, that they each play a different functional role in the perception of sound.

This study is concerned with modeling the response properties of cochlear-nucleus "stellate" cells (also described as multipolar cells, e.g., Hackney *et al.*, 1990). These cells are found predominantly in the anteroventral (AVCN) and the posteroventral (PVCN) divisions of the CN complex. Their afferents project directly to the nucleus of the lateral lemniscus, the superior olivary complex, deep regions of the dorsal CN and the inferior colliculus (Adams, 1979; Cant, 1982; Hackney *et al.*, 1990; Osen, 1972; Warr, 1982).

Stellate cells have several long dendrites that project from the soma at widely spaced angles (Brawer *et al.*, 1974; Hackney *et al.*, 1990). Many auditory-nerve (AN) fibers make synaptic contact with a cell forming small bouton terminals.

Two types of stellate cells can be distinguished in the AVCN based on whether the majority of synaptic connections on the cell are axosomatic or axodendritic. Cells that have more than 70% of the AN inputs on the cell dendrites are referred to as "type I," whereas cells that show the opposite pattern of AN innervation, i.e., more than 70% of inputs on the cell some are referred to as "type-II" units (Cant, 1981).

Cells with stellate morphology generally show a "chopper"-type post-stimulus time histogram (PSTH) response to short (< 50 ms) best frequency (BF), tone burst stimuli (Rhode *et al.*, 1983; Rouiller and Ryugo, 1984; Smith and Rhode, 1989). A typical chopper PSTH display shows a series of regularly spaced peaks of discharge that become less distinct after about 50 ms (Pfeiffer, 1966). The rate of chopping is typically unrelated to the frequency of the stimulus waveform.

Chopper-type neurons can be classified into a number of distinct subgroups including chop-S, chop-T, chop-W, and chop-LF (e.g., Bourk, 1976; Rhode and Smith, 1986; Young *et al.*, 1988a). One method of distinguishing between the various types of chopper neurons is known as regularity analysis (Bourk, 1976; Young *et al.*, 1988a; Blackburn and Sachs, 1989). Regularity measures are based on the variation in interspike intervals during the cell's response to tone bursts (see Sec. II for details). Chop-S units (regular choppers) have interspike intervals that remain constant over time, and chop-T units (one class of irregular choppers) have interspike intervals that increase over time. It is hypothesized that the anatomically defined type-I cells produce the physiologically defined chop-S response pattern and the type-II cells produce the chop-T response pattern (e.g., Blackburn and Sachs, 1989).

The proposed functional role of these two chopper sub-

 0001-4966/92/042096-14$00.80

types also differs. The chop-T units are implicated in the mechanism for the spectral encoding of perceptually important features of speech such as vowel formants. Physiological studies (Blackburn and Sachs, 1990) have demonstrated that chop-T neurons maintain a robust rate-place representation of vowel formants over a wide range of stimulus input levels. The same, however, does not apply to the chop-S neurons (Blackburn and Sachs, 1990). Instead, the chop-S neurons have been shown to encode the amplitude-modulation characteristics of an input signal, another perceptually important feature of speech sounds.

In this article, we concentrate on modeling the responses of the chop-S units. These cells preserve and even amplify the amplitude modulation (AM) characteristics of the stimulus over a wide range of input levels (Møller, 1976; Frisina *et al.*, 1990a,b; Kim *et al.*, 1990).

One of the most important features of the neural encoding of AM at the level of the CN is that each neuron produces maximal synchronization of firing at a particular rate of amplitude modulation while the average firing rate across modulation frequency remains relatively constant (Kim *et al.*, 1990). The exact mechanism for the preferential tuning of a chop-S neuron is unknown. It will be shown below that the model described in this article generates similar properties in response to AM stimuli. We describe the mechanism that generates these model responses.

We also show that the model is capable of replicating many of the physiological response properties of chop-S neurons. These include: (a) realistic onset and steady-state rate-level functions; (b) chopper-type post-stimulus time histogram responses; (c) typical chop-S type neuron responses characterized by a low coefficient of variance ($CV < 0.3$) of interspike intervals as a function of time; (d) level-dependent modulation transfer functions; (e) intrinsic oscillations in responses to pure-tone stimuli; (f) encoding of amplitude modulation over a wide dynamic range; and (g) frequency-limited phase locking.

The work of Frisina *et al.* (1990a) and Kim *et al.* (1990) has shown that chop-S neurons with common best frequencies (BFs) are preferentially tuned to a particular rate of amplitude modulation, such that at any one BF, there exists an array of neurons with systematically varied AM sensitivity.

Kim *et al.* (1990) have suggested that this arrangement of neurons could underlie a periodicity or pitch analysis at the level of the cochlear nucleus. A similar hypothesis has also been suggested by Langner and Schreiner (1988, Schreiner and Langner, 1988) for certain neurons in the central nucleus of the inferior colliculus based on a similar arrangement of neurons and response patterns.

It is intended that the model proposed here will provide the input to models of more central nuclei of the auditory brainstem such as the inferior colliculus. One of the aims of such work is to gain further insight into the possible neural mechanisms that underpin psychological phenomena such as pitch and auditory selective attention (Meddis, 1990).

The model we present here is similar in some respects to other models of chopper cells recently proposed (Arle and Kim, 1991; Banks and Sachs, 1991; Ghoshal *et al.*, 1990). Although each author takes a different approach to modeling stellate-cell responses, they all emphasize that the intrinsic properties of the cell membrane and dendritic processing are the central determinants of the *in vivo* response. The model presented here shows that such models are capable of generating a wide range of realistic stellate cell behavior in response to AM and pure-tone stimuli. One advantage of the current model is that it is based on a realistic simulation of the auditory periphery which is not constrained by the range or the type of input.

A flow diagram of the composite model used in this study is shown in Fig. 1. The model of the auditory periphery has been described in detail in previous publications (e.g., Meddis and Hewitt, 1991) and will be described only briefly. The stellate-cell model consists of two stages (Fig. 1, stages 6 and 7) which are described, and then developed according to the appropriate physiological data. Section II of the paper considers the response properties of the composite model to AM and pure-tone stimuli. Finally, Sec. III considers the effects of changing the model's parameters.

I. THE COMPOSITE MODEL

For the purpose of this study, all simulations were programmed in FORTRAN 77 on a Masscomp 5450 computer. The step integration size (dt) was 20 μs (50-kHz sample rate).

A. Simulation of the auditory periphery

To compare the response properties of the stellate-cell model to neural responses from animal preparations, we

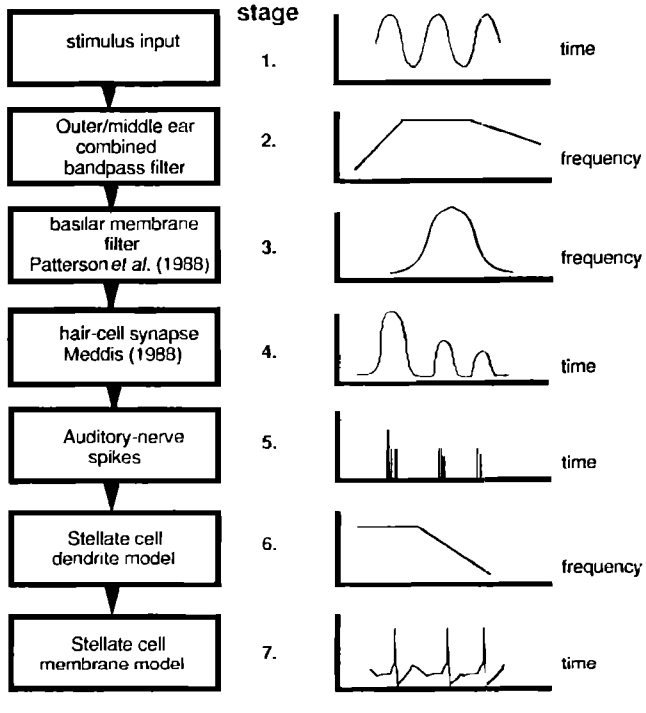

FIG. 1. The processing sequence of the model (see text for details).

needed to simulate, as close as possible, normal input to the stellate cell from the auditory nerve. For this purpose, we used the peripheral model developed in our laboratory (Meddis and Hewitt, 1991) to provide the input to the stellate-cell model.

The stages of the peripheral model are summarized below.

(1) Stimulus generation: Stimulus parameters varied with the experimental paradigm and are specified in Sec. II.

(2) Outer-ear/middle-ear, low- and high-frequency attenuation: Outer/middle ear effects are combined to produce an attenuation of frequencies below 1 kHz and above 5 kHz.

(3) Inner-ear, cochlear mechanical filtering of the basilar membrane: This was implemented using a single linear bandpass digital filter (Patterson *et al.*, 1988). The required channel is specified by its center frequency. Unless stated otherwise, the center frequency of the channel was 5 kHz.

(4) Mechanical to neural transduction at the inner-hair cell/auditory-nerve synapse: This was implemented using the computer model proposed by Meddis (1986, 1988; Meddis *et al.*, 1990). The model replicates a number of auditory-nerve response properties such as two-component adaptation, half-wave rectification, and frequency-limited phase locking. The relative merits of this and seven other hair-cell models are discussed in Hewitt and Meddis (1991). The output of this stage is expressed as the probability of occurrence of a spike in the auditory-nerve fiber of the 5-kHz channel.

The parameters of the hair-cell model were set to simulate the characteristics of a high spontaneous rate fiber (Table I). This yields a fiber with a spontaneous rate of about 35 spikes/s, a saturated rate of about 150 spikes/s, and a limited (30 dB) dynamic range.

(5) Auditory-nerve spike generation and refractory effects: Refractory inhibition of firing of the auditory nerve was computed as an adjustment to the hair cell firing probability as a function of time since it last generated a spike (see Meddis and Hewitt, 1991 for details). Individual AN spikes were generated from the hair-cell firing probability using pseudorandom number techniques (e.g., Hastings and Peacock, 1975, p. 41). The output of this stage represents the number of active auditory-nerve fibers per time unit simulated. Unless stated otherwise, 60 auditory-nerve fiber inputs were simulated.

TABLE I. Hair cell model parameters.

Parameter	
A	5
B	800
g release	1000
y replenish	5.05
l loss	1250
r recovery	6580
x reprocessing	66.31
Properties	
Spontaneous rate (sp/s)	35
Saturated rate (sp/s)	150
Dynamic range (dB)	30
Synchronization index (1 kHz)	0.9
Synchronization index (5 kHz)	0.62

B. Cell-soma model

The cell-soma model to be described was based on a digital simulation of the Hodgkin and Huxley conception of spike generation (MacGregor, 1987, point-neuron 10, p. 458; see also Arle and Kim, 1991). Briefly, this point-neuron model produces relatively realistic ongoing input–output dynamics for a neuron with basic accommodative properties. Because there are numerous minor changes to the model, it will be presented again here in full.

The model is activated by a single input function that represents the stimulating current from an experimentally applied electrode. The model is characterized by four variables: (1) the transmembrane potential measured as a deviation from the cell resting potential; (2) a potassium conductance; (3) the time-varying threshold; and (4) an all-or-nothing spiking variable.

Changes in these variables are governed by four differential equations. The first describes the change in the transmembrane potential in response to input current:

$$\frac{dE(t)}{dt} = \frac{-E(t) + \{V(t) + G_k(t)[E_k - E(t)]\}}{\tau_m}, \tag{1}$$

where $E(t)$ is the instantaneous cell-membrane potential above resting level E_0, $G_k(t)$ is the instantaneous cell potassium conductance, τ_m is the membrane time constant, E_k is the equilibrium potential of potassium conductance relative to cell resting level, and $V(t)$ is the instantaneous change in potential resulting from applied or synaptic current.

The equation describing the potassium conductance is as follows:

$$\frac{dG_k(t)}{dt} = \frac{-G_k(t) + (bs)}{\tau_{Gk}}, \tag{2}$$

where b is the delayed rectifier potassium conductance strength, s is the spiking variable (0 or 1), and τ_{Gk} is the time constant of potassium conductance decay.

The model includes a term for accommodation whereby a cell's firing threshold varies as a function of simulation. The equation describing the rise in threshold is as follows:

$$\frac{d\,\mathrm{Th}}{dt} = \frac{-[\mathrm{Th}(t) - \mathrm{Th}_0] + cE(t)}{\tau_{\mathrm{Th}}}, \tag{3}$$

where $\mathrm{Th}(t)$ is the time-varying threshold of the cell, Th_0 is the resting threshold of the cell, c is the accommodation constant, and τ_{Th} is the time constant of threshold rise.

The main output function is a combination of the transmembrane potential and the spiking variable

$$p(t) = E(t) + s[E_b - E(t)], \tag{4}$$

where E_b is the reversal potential of the cell, $s = 0$ if $E(t) < \mathrm{Th}$, and $s = 1$ if $E(t) > \mathrm{Th}$.

When cells are depolarized or hyperpolarized with current, the consequential potential change is proportional to

the magnitude of the injected current. The constant of proportionality is known as the "input resistance" of the cell. That is,

$$V(t) = I_s(t)R_i, \tag{5}$$

where $V(t)$ is the instantaneous magnitude of cell membrane potential change, $I_s(t)$ is the instantaneous magnitude of the current applied to the cell soma, and R_i is the input resistance of the cell.

1. Development of the soma model

To develop the cell-soma model, we used stellate cell data collected from the *in vitro* work of Oertel (1983, 1985; Oertel *et al.*, 1988) to specify the parameters of the model.

Oertel demonstrated that the chopper firing pattern of VCN stellate cells *in vivo* was due, in part, to their intrinsic membrane conductances. They made intracellular recordings from slices of cochlear nuclei maintained *in vitro*. Oertel studied the intrinsic electrical properties of stellate cells by measuring responses to injected depolarizing and hyperpolarizing current pulses of different magnitudes.

The essential features of *in vitro* stellate cell responses are: (a) an approximately linear current–voltage relationship in the subthreshold range, (b) depolarization past firing threshold results in action potentials whose peaks approach 0 mV, (c) within physiological limits, the greater the depolarization, the faster the cell fires, (d) a single hyperpolarizing peak follows the downstroke of each action potential, and (e) hyperpolarizing current pulses produce almost exponential changes in membrane potential at onset and offset.

Using the modified point-neuron program described above with the parameters listed in Table II, we have replicated (qualitatively at least) all of these characteristics. Some of the parameters (e.g., initial threshold, Th_0; input resistance, R_i; membrane time constant, τ_m) were specified by Oertel's data whereas others were derived empirically to give the best fit results.

Figure 2 shows model and experimentally observed (Oertel, 1983) cell responses to depolarizing and hyperpolarizing current pulses of equal magnitude. Figure 3 shows the input–output function of the model compared with data from Oertel (1983).

The main features of the model behavior can be explained as follows. With a relatively fast membrane time

TABLE II. Model parameter values for stellate-soma model.

Parameter	Model	Unit
c	0.3	dimensionless
τ_{TH}	20.0	ms
b	0.017	ns
τ_{Gk}	0.9	ms
TH_0	10.0	mV
τ_m	2.0	ms
R_i	33.0	mΩ
E_b	0.0	mV
E_0	− 60.0	mV

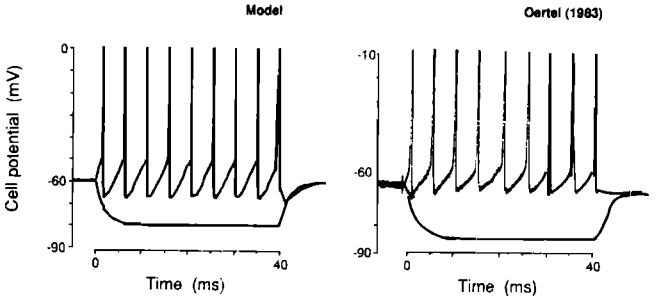

FIG. 2. Model and neural responses (Oertel, 1983, Fig. 5) to depolarizing and hyperpolarizing current pulses of 0.6 nA.

constant, the cell potential rises rapidly when driven by the depolarizing pulse and soon reaches firing threshold. This gives rise to the first action potential. The parameters τ_{Gk} and b determine the rate of recovery of the cell back to resting potential following the downstroke of each spike. These parameters were set to give a fast recovery in order to simulate Oertel's data. In this version of the model, the firing threshold varies only slowly over time; thus the membrane potential quickly returns to firing threshold and another action potential is triggered.

We found that the frequency of firing could be adjusted by changing either the potassium conductance (τ_{Gk},b), or the membrane time constant (τ_m), or the accommodation term (c). Later we change the parameter τ_{Gk} to simulate the neural data from *in vivo* studies.

C. The cell-dendrite model

1. Spatial convergence

Morphological studies (e.g., Cant and Morest, 1984) have shown that many auditory-nerve fibers converge onto

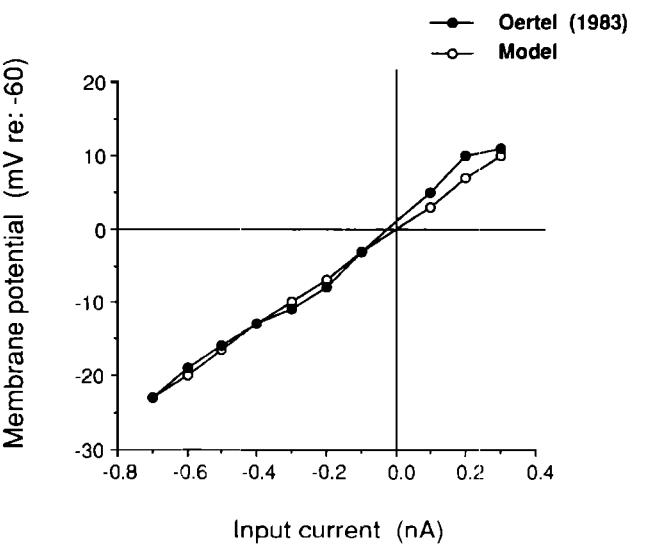

FIG. 3. Model (open circles) and neural (closed circles) subthreshold current-voltage functions (neural data redrawn from Oertel, 1983, Fig. 5).

the dendrites of a single stellate cell. Moreover, Oertel (1985) has demonstrated that stellate cells integrate spike activity from the array of auditory-nerve fiber inputs.

Oertel's method was to apply brief electrical shocks (0.1 ms) to the cut end of the auditory nerve and record the changes in the membrane potential of electrode-impaled VCN cells. When low-voltage shocks were applied to the auditory-nerve stump, they recorded only small subthreshold excitatory post-synaptic potentials (EPSPs) in the stellate cell. With high-voltage shocks, the EPSPs became suprathreshold and the cell elicited a spike. Oertel showed that the amplitude of EPSPs was a graded function of the voltage at which the auditory nerve was stimulated, and concluded that as the shock voltage increased more and more auditory-nerve fibers were recruited and increased the post-synaptic effect. This effect is known as "spatial summation."

In the model, we approximate this process by performing a linear summation of all simultaneous inputs to the cell. We model a number of auditory-nerve fibers all of which contact the dendrites of a single stellate cell. Each spike from each auditory-nerve fiber depolarizes the stellate cell dendritic tree, such that the total current delivered to the cell is

$$I_d(t) = n(t)\Delta I, \tag{6}$$

where $I_d(t)$ is the instantaneous magnitude of dendritic current, $n(t)$ is the instantaneous number of spiking AN fibers (the output of the peripheral model), and ΔI is the current per AN spike.

For convenience, we limited the total amount of current that could be delivered to the cell, but varied the total number of auditory-nerve fibers that contacted the cell. Thus, the current per auditory-nerve spike was calculated as follows:

$$\Delta I = I_{\max}/N, \tag{7}$$

where $I_{\max}$ is the maximum current that could be delivered to the cell, and N is the number of auditory-nerve fibers contacting the cell.

2. Low-pass dendritic filtering

Morphological studies (e.g., Cant, 1979; Smith and Rhode, 1989) show that the terminals of auditory-nerve fibers synapse predominantly on the dendrites of type-I(chop-S) cells with very few synaptic somatic connections. These features have important implications for the transmission of the input signal from the synapse to the soma of the cell where the output spikes are generated. If it is assumed that the spread of current down the dendrite to the soma is a passive process then the signal at the soma will be attenuated compared to the signal at the dendrite.

This principle is taken from the domain of cable theory (e.g., Rall, 1989). The theory established that for passive conduction of current through a cable, the amplitude of the signal falls off exponentially with increasing distance from the source. Application of the theory to neural models have found that the signal at the soma is a low-pass filtered version of the input signal. The effects of the filtering become increasingly significant as the distance between source and soma increases.

Detailed modeling of these effects have been reported by Young *et al.* (1988b) and by Banks and Sachs (1991) using a compartmental model of dendritic processes. Based on the parameters of cat spinal motor neurons, Young *et al.* (1988b) calculated that a 1-kHz signal applied at the end of a dendritic tree could be attenuated by as much as 60 dB when measured at the soma. However, the data of Smith and Rhode (1989) show that the majority of synapses of type-I stellate cells are within 100 μm of the soma. The implication is that in this case the effect of low-pass filtering would not be as severe as that calculated by Young *et al.* (1988b).

For the purpose of the model, we have approximated the effects of dendritic filtering by low-pass filtering the total current applied to the cell. This was achieved with a simple first-order Butterworth filter designed to give 6-dB attenuation per octave. (Beauchamp and Yuen, 1979). The filter is specified as follows:

$$I_s(t) = GI_d(t) + GI_d(t - dt) - HI_s(t - dt), \tag{8}$$

where $I_d(t)$ is the instantaneous magnitude of dendritic current [see Eq. (6)], $I_s(t)$ is the instantaneous magnitude of the current applied to the cell soma,

$$G = 1/[1 + 1/\tan(\pi f_c\, dt)], \tag{9}$$

$$H = \{1 - [1/\tan(\pi f_c\, dt)]\}/\{1 + [1/\tan(\pi f_c\, dt)]\}, \tag{10}$$

$$dt = 1/\text{sample rate}, \tag{11}$$

and f_c is the filter cutoff frequency (Hz).

a. Development of the dendrite model. Oertel (1985) demonstrated that stellate cells maintained *in vitro* showed both spatial and temporal summation. The method was to apply brief electrical shocks (0.1 ms) to the cut end of the auditory nerve and record the changes in the membrane potential of electrode-impaled VCN cells.

To simulate the method of Oertel, we presented clicks (0.1-ms duration) to the model auditory-nerve fibers that produced subthreshold and suprathreshold responses in the VCN cell. The results together with Oertel's (1985) data are shown in Fig. 4(a). The model reproduces Oertel's results qualitatively. At low click levels, the AN firing probability is low which gives rise to only a small number of synchronous AN firings. Thus the total current delivered to the stellate cell is not sufficient to raise the cell's membrane potential above firing threshold. At higher click levels, the AN firing probability is high which gives rise to a large number of synchronous AN firings. In this case, the summed synaptic drive is sufficient to elicit a spike from the stellate cell.

It should be noted that although the shape and duration of the model's action potentials are somewhat different from those measured empirically. However, it is unlikely that this would influence the nature of the results presented below because the shorter action potential produced by the model is counterbalanced by the duration of the post-spike hyperpolarization.

In general, Oertel was unable to estimate the number of auditory-nerve inputs contributing to the responses of the stellate cells. Explorations of the model's properties were conducted by varying the number of auditory-nerve fibers. These results are presented in Sec. III.

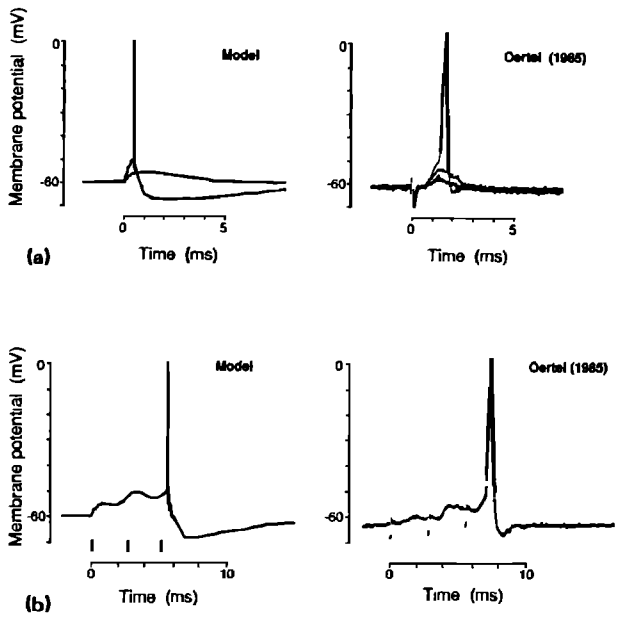

FIG. 4. (a) Model and neural data in response to "shocks" presented to the auditory nerve that produce subthreshold and suprathreshold responses in stellate cells. Neural data redrawn from Oertel (1985, Fig. 4). (b) Model and neural data in response to shock stimuli (0.1-ms duration) presented to the auditory nerve at a rate of 360/s. Neural data redrawn from Oertel (1985, Fig. 4).

The effect of dendritic filtering gives rise to the phenomena of "temporal summation." That is, the effects of an incoming auditory-nerve spike are not simply instantaneous but continue to influence the dendritic membrane for some time after the spike. This feature has been demonstrated in stellate cell responses recorded by Oertel (1985; Oertel *et al.*, 1988). Oertel showed that when the stump of the auditory nerve was stimulated repetitively at a low-voltage level, subthresold EPSPs summed in time to become suprathreshold eliciting an action potential.

Figure 4(b) shows the model responses to subthreshold clicks at a rate of 360 per second together with data redrawn from Oertel (1985). From the data presented, Oertel concluded that the EPSPs must be longer than 2.6 ms in order to sum in time. In the model, the low-pass filter largely determines the shape and duration of the soma EPSP. The best simulation results were obtained with the filter cutoff frequency at 300 Hz. The choice of the filter cutoff frequency will be discussed later.

The summing of synaptic responses in time and space sometimes obscures the relationship of the fine-time structure of the cell's responses to the stimulus. The stimulus parameters of rate and strength seem to be crucial. For example, when the rate of stimulation is relatively slow and the strength of shock is suprathreshold, a stellate cell will preserve the temporal firing pattern of its input, but not otherwise (see Fig. 10, Oertel *et al.*, 1988).

II. EVALUATION OF THE COMPOSITE MODEL

A variety of stimulus paradigms and spike analysis techniques have been employed by the physiologist to characterize the response properties of stellate cells. In this section, we evaluate the composite model by comparing model responses to neural stellate cell data. All the simulation data reported in this section were generated from the model using a single parameter set. The parameter values are as listed in Table II except that τ_{Gk} was changed from 0.9 to 2.05 ms. The main effect of this change was to decrease the intrinsic firing rate of the model cell.

A. Rate-level functions

In the absence of sound stimulation, stimulation stellate cells fire spontaneously at low rates (< 10 spikes/s). In response to sound, the steady-state rate increases almost monotonically over a 20-dB range before saturating (Bourk, 1976; Godfrey *et al.*, 1975; Møller, 1974; Frisina *et al.*, 1990b). In addition, Frisina *et al.* (1990b) measured onset rate-level functions. In common with primary-afferent data, typical stellate-cell onset functions showed a greater dynamic range than the steady-state function.

Figure 5 shows the model rate-level functions in response to a 5-kHz BF tone compared to data of Frisina *et al.* (1990b, Fig. 1a, unit 74). The essential features of the neural functions are matched at least qualitatively by the model. The stellate-cell model has a spontaneous rate of 0.2 spikes/s. The rate-level functions enabled us to establish a reference level for the model. For the purpose of this work, 0 dB was defined as the level at which the onset and steady-state rate-level functions started to diverge. All stimulus input levels quoted in this paper should be read as dB *re*: reference level.

B. Post-stimulus time histogram response

The temporal responses of cochlear nucleus cells to tone burst stimuli are usually classified according to the scheme of Pfeiffer (1966). Cells with "stellate" morphology generally show a "chopper" PSTH response (Rhode *et al.*, 1983;

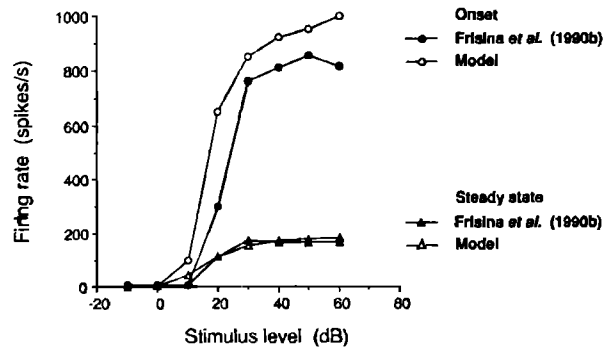

FIG. 5. Model (open symbols) and neural (closed symbols) rate-level functions. Stimulus input levels are dB *re*: unit threshold. Stimulus repetitions: 40. The onset function (circles) represents the maximal firing rate during the first (or highest) ms window of response at stimulus onset. The steady-state function (triangles) represents the average firing rate over a 20-ms period, 25 ms after stimulus onset. Neural data redrawn from Frisina *et al.* (1990b, Fig. 1a).

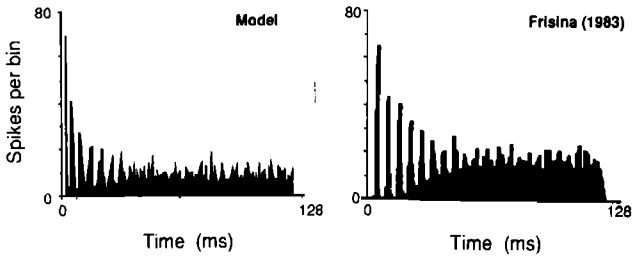

FIG. 6. Model and neural PSTHs from responses to 128-ms duration BF pure tones. Model parameters: Stimulus input level: 32 dB, histogram bin width: 0.64-ms, stimulus repetitions: 80. Neural data redrawn from Frisina (1983, Fig. 7b).

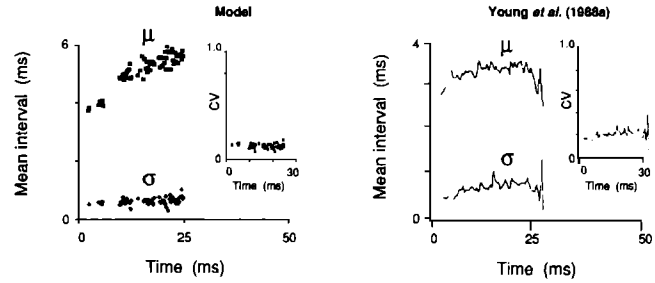

FIG. 7. Regularity analysis on model and neural PSTHs. See text for details. Model parameters: stimulus input level: 30 dB, 50-ms duration pure tone of 5-kHz, stimulus repetitions: 500, bin width: 0.2 ms. Histogram bins with less than 3 spikes are not plotted. Neural data redrawn from Young *et al.* (1988a, Fig. 2B).

Rouiller and Ryugo, 1984). Chopper PSTHs show a series of regularly spaced peaks of discharge that become less distinct after about 50 ms. The rate of "chopping" is typically unrelated to the frequency of the stimulus waveform.

Figure 6 shows the model PSTH in response to a 5-kHz tone burst of 128-ms duration presented at 32 dB and is compared to the data of Frisina (1983, Unit 35, level 32 dB).

C. Regularity/interspike interval analysis

Chopper-type neurons can be classified into a number of distinct subgroups using regularity analysis techniques (Bourk, 1976; Young *et al.*, 1988a; Blackburn and Sachs, 1989). Regularity is measured by estimating the mean (μ_R) and standard deviation (σ_R) of interspike intervals as a function of time during responses to tone bursts. The coefficient of variation ($CV = \sigma_R/\mu_R$) is used as a measure of irregularity, where an increase in CV equates to an increase in irregularity. The technique gives a sensitive and stable characterization of units' responses.

Young *et al.* (1988a) noted at least two distinct chopper populations using CV measures: chop-S (sustained) units are regular choppers with CVs less than 0.3 that show only slight variation over time; chop-T units (transient) are irregular choppers and have CVs greater than 0.3 and show an increase in irregularity over time.

Figure 7 shows the mean (μR) and standard deviation (σR) of interspike intervals as a function of time during model responses to a 5-kHz tone burst of 50-ms duration (regularity data calculated over the first 25 ms), compared to data from Young *et al.* (1988a). The mean CV measured between 15 and 20 ms post-stimulus onset is 0.12 which is typical of chop-S neural data.

D. Modulation transfer functions

Amplitude modulation is a simple type of dynamic stimulus that plays a key role in a variety of auditory phenomena. Following the pioneering work of Møller (1972, 1973, 1976) other studies have shown that the amplitude-modulation characteristics of a signal are enhanced by certain cells in the VCN (Frisina *et al.*, 1990a; Kim *et al.*, 1990).

Frisina *et al.* (1990a) examined the enhancement of responses to amplitude modulation in single neurons of the gerbil VCN. The majority of units in Frisina's study were classified as chop-S neurons. To quantify the enhancement of amplitude modulation, Frisina calculated the modulation gain for each neuron in response to BF tones amplitude modulated over a range of low frequencies (25–1000 Hz).

Modulation gain (in dB) is calculated as follows:

$$\text{modulation gain} = 20 \log_{10}(r_h/r_s), \tag{12}$$

where r_h and r_s are the vector strengths (Goldberg and Brown, 1969) of the response period histogram and the input stimulus, respectively.

Vector strength is calculated as

$$r = \frac{\sqrt{\left[\Sigma_0^{K-1} R_k \cos 2\pi(k/K)\right]^2 + \left[\Sigma_0^{K-1} R_k \sin 2\pi(k/K)\right]^2}}{\Sigma_0^{K-1} R_k}, \tag{13}$$

where K is the number of bins in the period histogram, and R_k is the magnitude of the k th bin.

1. Level dependence

Neural modulation transfer functions (MTFs, modulation gain plotted against modulation frequency) are *low pass* for stimulus levels below 20 dB (*re*: threshold) and narrowly tuned *bandpass* functions for levels above this. Frisina *et al.* (1990a) noted that the peak-modulation gain was maximal at 30 dB then decreased on average by about 5 dB for stimulus-input levels between 30 and 50 dB.

Using our composite model, we replicated (qualitatively at least) the main features described above.[1] Figure 8(a)

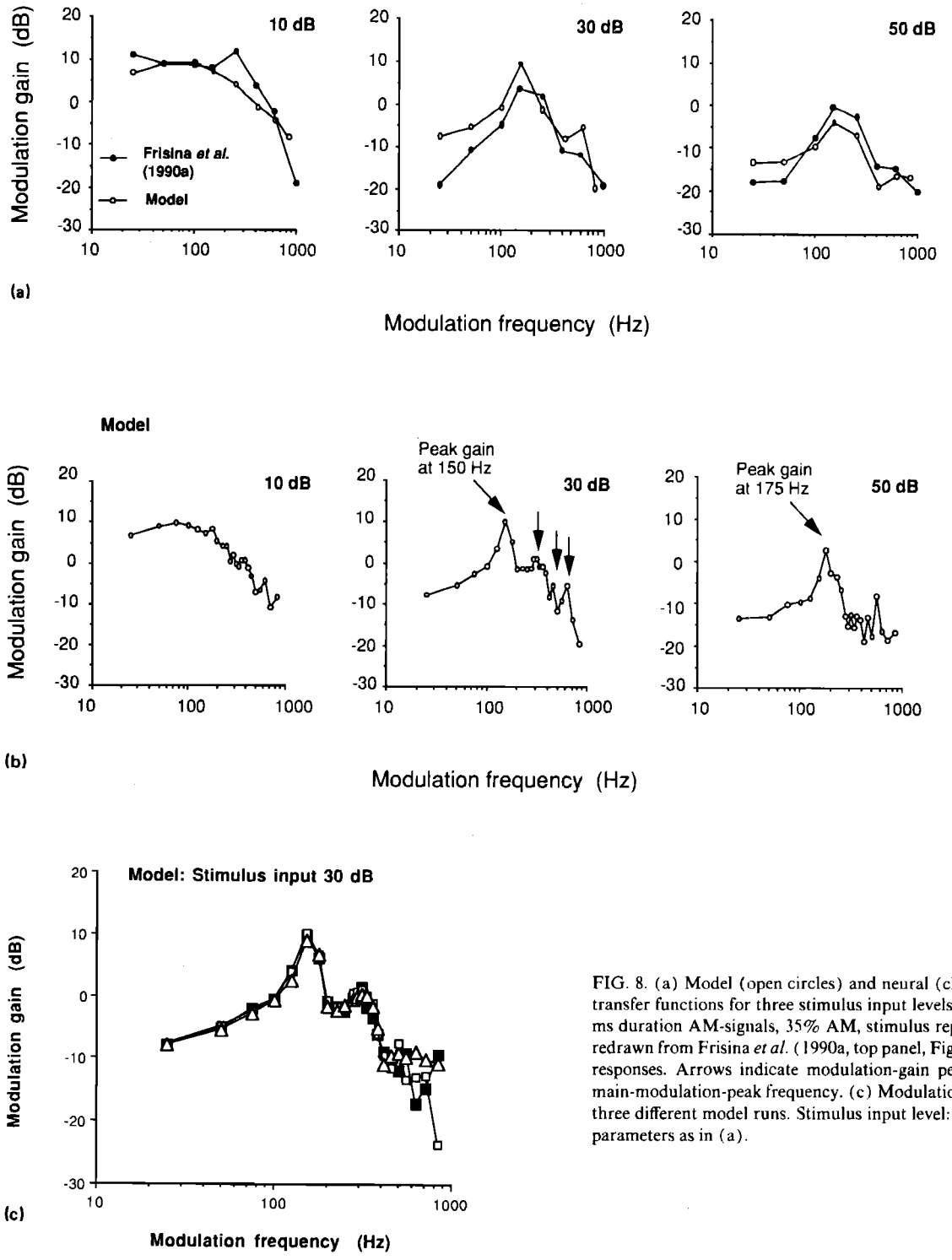

FIG. 8. (a) Model (open circles) and neural (closed circles) modulation transfer functions for three stimulus input levels. Model parameters: 200-ms duration AM-signals, 35% AM, stimulus repetitions: 40. Neural data redrawn from Frisina *et al.* (1990a, top panel, Fig. 12). (b) Detailed model responses. Arrows indicate modulation-gain peaks at harmonics of the main-modulation-peak frequency. (c) Modulation transfer functions from three different model runs. Stimulus input level: 30 dB, all other stimulus parameters as in (a).

shows MTFs derived from model responses to a 5-kHz tone which was amplitude-modulated over a range of frequencies for three different input levels. The figure shows the data of Frisina superimposed for comparison (redrawn from Frisina *et al.*, 1990a, Fig. 12, unit 131). The model replicates the main qualitative features of the neural MTFs, namely; a low-pass function at low stimulus levels, bandpass functions at high stimulus levels, and a reduction in the peak modulation gain as input level increases. The frequency of peak modulation gain could be changed by varying the parameter τ_{Gk}. In the case of Fig. 8(a), where τ_{Gk} was set at 2.05 ms, the peak modulation gain was at about 150 Hz.

Kim *et al.* (1990) mapped the MTFs of dorsal CN (DCN) and PVCN neurons in unanesthetized decerebrate cats. They observed MTFs qualitatively similar to those of Frisina's study but, noted a small upward shift in peak modulation frequency as stimulus level increased. We ran the model with the same stimulus paradigm as above but with

greater modulation frequency resolution. Figure 8(b) shows the model responses. We can see that the model peak-modulation-gain frequency increased by about 25 Hz as the stimulus input level increased from 30 to 50 dB. This compares very favourably to the data reported by Kim *et al.* (1990).

2. Subsidiary best-modulation frequency peaks

Figure 8(b) also shows that at moderate input levels (30 dB) the model predicts subsidiary peaks of modulation gain at approximately two, three, and four times the main modulation-peak frequency. Three different model runs are shown in Fig. 8(c) for the 30-dB input level. In each case there is a clear subsidiary peak at twice the frequency of the main peak. Further peaks at multiples of the main peak frequency are not always clearly defined. Unfortunately, as the studies of both Frisina *et al.* (1990b) and Kim *et al.* (1990) used only a relatively small number of modulation frequencies to map out each transfer function, subsidiary modulation-gain peaks may have been missed. However, in the case of the secondary peak, the model prediction is clear and robust and will hopefully guide future physiological experimentation to decide the issue.

3. Response to the fundamental-frequency component

Kim and his colleagues (1990) noted that the enhancement of AM was manifest in the synchronized rate response to the fundamental frequency (f_0) of the AM complex. While the average rate response of a neuron remained constant over modulation frequency, the f_0 response varied with the modulation frequency of the input. In the case of a neuron with bandpass-shaped MTF, the peak fundamental rate response corresponded to the frequency of the peak modulation gain.

Figure 9 shows that the response component of the model to the fundamental frequency of the stimulus varied systematically with the modulation envelope frequency. In contrast, the average response rate is independent of modulation envelope frequency. That is, the model achieves an enhancement of modulation by an increase in the synchronization of

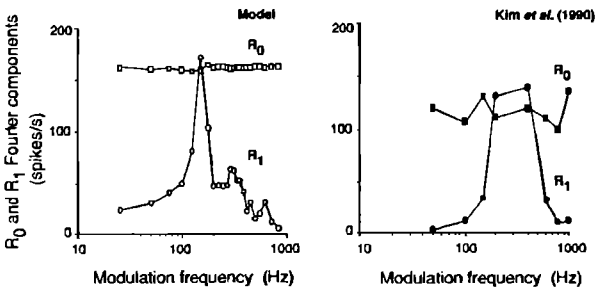

FIG. 9. Model and neural firing rate responses to AM-stimuli. The total response (R_0, spikes/s) are shown as squares and the response to the fundamental-frequency component (R_1, spikes/s) of the signal are shown as circles. Model parameters: stimulus input level 30 dB, 35% AM, 200-ms duration, stimulus repetitions: 40. Neural data from Kim *et al.* (1990, bottom panel, Fig. 2).

firing to the f_0 component of the stimulus. The model results are very similar to the neural data (Kim *et al.*, 1990, redrawn in Fig. 9). One discrepancy between the model and neural data concerns the width of the increased response to the f_0 component of the stimulus. The model predicts a clear peak of response, whereas the neural function is flat topped spanning a range of about 300 Hz. We have no explanation for this discrepancy.

E. Intrinsic oscillations

Kim *et al.* (1990) analyzed the responses of DCN-PVCN neurons to pure-tone signals with autocorrelation and power spectra. The authors' rationale for use of the techniques was to provide a complete description of the frequency components of a neuron's response. They found that a CN neuron's response to pure-tone stimuli often exhibited intrinsic oscillations in the patterns of spike discharges. The intrinsic oscillations were in general not related to the frequency of the signal but reflect constant properties of the cell itself. Consequently, a period histogram, or even its power spectrum would not detect the intrinsic oscillation of a particular neuron.

As noted above, Kim classified DCN-PVCN neurons into one of two types according to their modulation transfer function; low-pass or narrowly tuned bandpass. Analysis with autorcorrelation and power spectra showed that neurons with bandpass functions exhibited intrinsic oscillations, whereas the low-pass neuron types did not. As shown earlier the modulation transfer characteristic of our model neuron was bandpass. Following the method of Kim and his colleagues we analyzed the model responses for the presence, or otherwise, of intrinsic oscillations.

The responses of single DCN-PVCN (bandpass MTF) neurons to high-frequency (>5 kHz) pure tones analyzed with power spectra techniques exhibited response components at the cell's intrinsic oscillation frequency. Smaller response components at the second and third harmonics of the intrinsic oscillation were also present. No response component was present at the frequency of the tone as auditory-nerve phase locking declines at frequencies above 4–5 kHz (Rose *et al.*, 1967). Consequently, the temporal information concerning the carrier frequency of a high-frequency signal is not conveyed to the cochlear nucleus neurons.

Figure 10 shows the model data derived from responses to a 5-kHz tone burst of 800-ms duration. The figure is a plot of the power spectrum of an autocorrelation of model spike trains in response to the tone. The main features of the neural data are replicated. No response component was present at the frequency of the one due to the breakdown of phase locking at high frequencies imposed by the hair-cell model (Meddis, 1986, 1988; Meddis *et al.*, 1990).

F. Encoding of AM over a wide dynamic range

Møller (1972, 1976), Frisina *et al.* (1985), and Kim *et al.* (1990) showed that cochlear nucleus units had wider dynamic ranges than auditory-nerve fibers for AM encoding. For example, Kim *et al.*, found that most AN fibers had dynamic ranges for AM encoding in the region of 20–40 dB

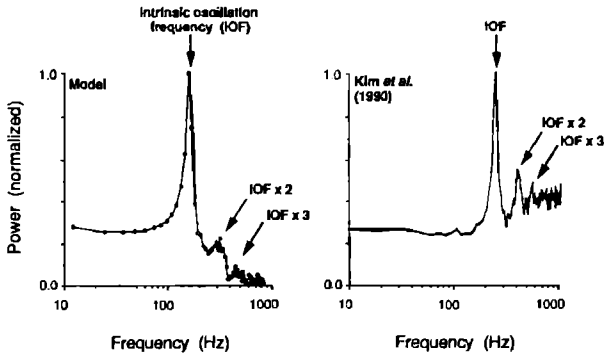

FIG. 10. Model and neural intrinsic oscillations. Each panel shows the normalized power spectrum of autocorrelated spike trains in response to BF tones. Arrows indicate response components at the harmonics of the cells intrinsic oscillation frequency. Model parameters: input level: 50 dB, duration: 0.8 s, stimulus repetitions: 40. Neural data redrawn from Kim *et al.* (1990, Fig. 6d).

while the majority of PVCN neurons had ranges in excess of 40 dB. Using the methods of Kim *et al.*, we measured the dynamic ranges of AM encoding in the model. In agreement with the neural data, AM encoding at the level of the auditory-nerve model extended over a 30-dB dynamic range while the output of the model stellate-cell showed a 40-dB range.

G. Frequency-limited phase locking

Winter and Palmer (1990) measured the decline of phase locking in AVCN chopper cells of the guinea pig in response to low-frequency pure tones. They quantified the responses with the vector strength or synchronization index (SI) metric (Goldberg and Brown, 1969; Johnson, 1980). They found that phase locking started to decline at 200 Hz (SI = 0.8) and was almost absent at 1.5 kHz (SI = 0.1). The model data together with Winter and Palmer's data from their chop-S units are shown in Fig. 11. The model data are quantitatively correct.

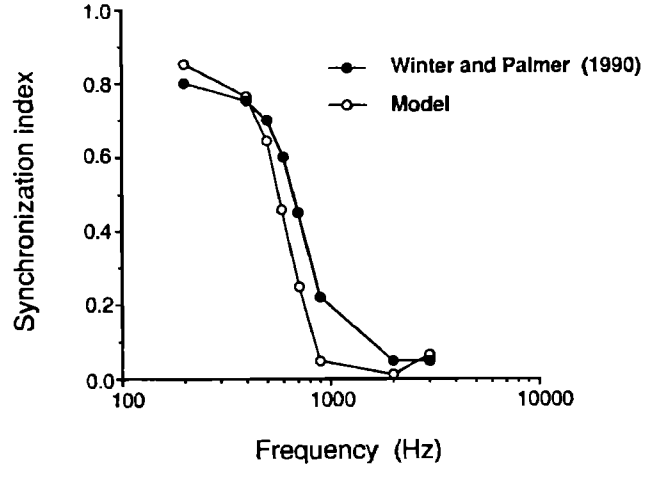

FIG. 11. Model (open circles) and neural (closed circles) synchronization indices. Model parameters: stimulus duration: 200 ms, repetitions: 40. Neural data (averaged and) redrawn from Winter and Palmer (1990, Fig. 11c).

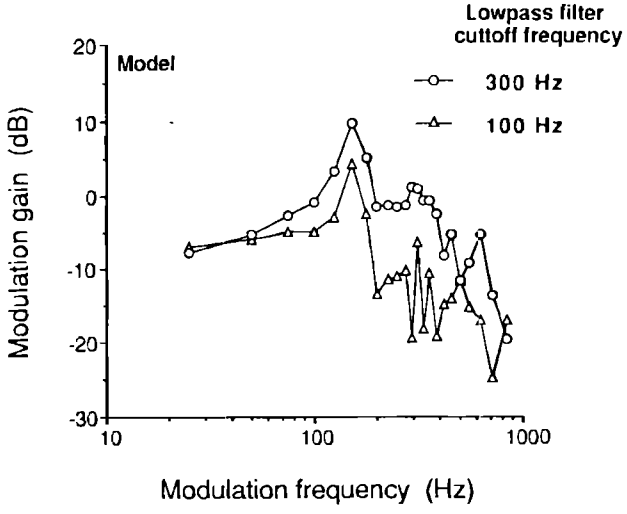

FIG. 12. Effect of low-pass filter cutoff frequency on model modulation transfer functions. AM-signals presented at 30 dB, 35% AM, 200-ms duration, stimulus repetitions: 40. Cutoff frequency, f_c = 300 Hz (circles): f_c = 100 Hz (triangles).

III. EFFECTS OF CHANGING MODEL PARAMETERS

We consider the effects of changing the low-pass filter cutoff frequency, and the number of auditory-nerve fibers used in the model. Details of changing the parameters of the stellate cell soma model we noted in Sec. I. Full details of changing the hair-cell model parameters are presented in Meddis *et al.* (1990).

Figure 12 shows model modulation transfer functions (input level 30 dB) with the low-pass filter cutoff frequency reduced from 300 to 100 Hz. The main qualitative features of

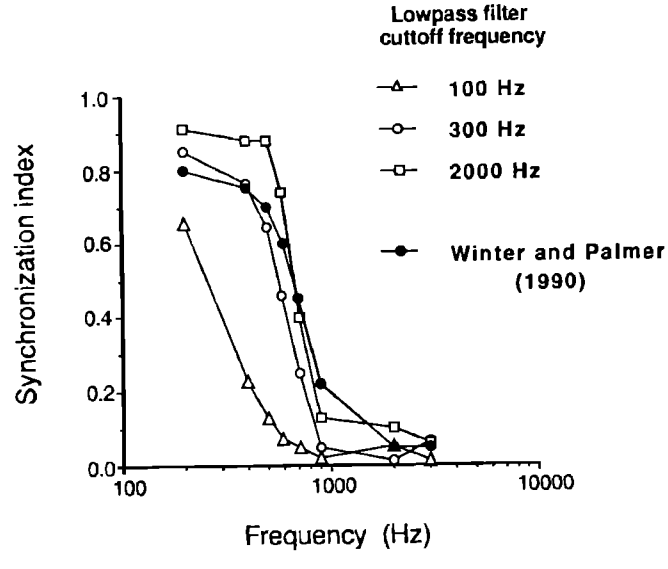

FIG. 13. Effect of low-pass filter cutoff frequency on model synchronization. Model parameters: stimulus duration: 200 ms, repetitions: 40. Cutoff frequency, f_c = 300 Hz (open circles); f_c = 100 Hz (open triangles); f_c = 2000 Hz (open squares). Neural data (closed circles) from Winter and Palmer (1990, Fig. 11c).

neural MTFs are maintained. However, lowering the filter cutoff frequency did have an effect on the model's synchronization responses to low-frequency tones as is shown in Fig. 13. The fall-off in synchrony is too severe. Increasing the filter cutoff frequency had little effect on the model's synchronization responses to low-frequency pure tones (Fig. 13) suggesting that the dendritic filtering plays only a small part in determining stellate cell synchronization to pure tones. However, increasing the cutoff frequency above about 1 kHz produced only short EPSPs and the model lost the ability to summate subthreshold temporal information (see Sec. I).

The effect of reducing the number of AN-fiber inputs converging on the model dendrite was to increase the irregularity of the model responses [the mean input was kept constant, see Eq. (7)]. Figure 14 shows the model MTFs from simulations was 5, 30, and 60 AN fibers. As the number of fibers decreased so the peak modulation gain decreased such that with only 5 AN fibers the 30-dB MTF is more low pass than band pass in shape.

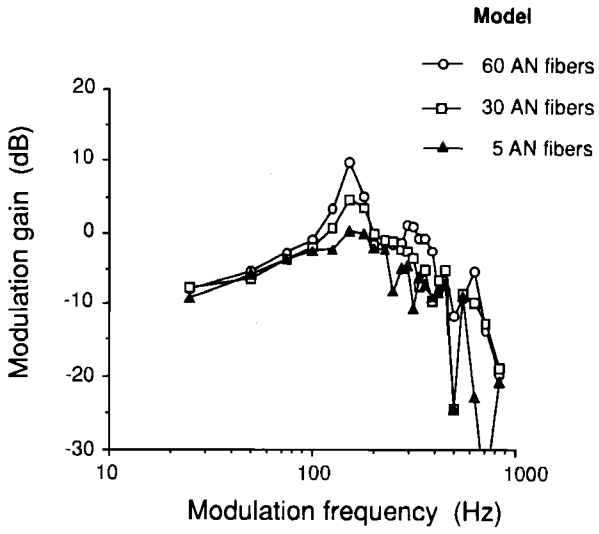

FIG. 14. Effect of number of AN fibers on model MTFs. AM-signals presented at 30 dB, 35% AM, 200-ms duration, stimulus repetitions: 40. Number of AN fibers, $N = 60$ (circles); $N = 30$ (squares), and $N = 5$ (triangles).

IV. DISCUSSION

We have presented and evaluated a computer model of a CN stellate neuron. The core component of the model is a series of equations designed to simulate the change in a cell's membrane potential in response to depolarizing and hyperpolarizing current pulses. Using this model, we were able to replicate the typical input–output functions of stellate cells maintained *in vitro* (Oertel, 1983, 1985; Oertel *et al.*, 1988).

We then simulated the low-pass filtering effect of stellate-cell dendrites. The development of this stage was guided, in part, by the morphological studies of Cant and Morest (1984). Their work showed that stellate cells have a number of long dendrites upon which many auditory-nerve fibers may synapse. This feature of stellate-cell morphology leads to a progressive attenuation of the signal as it travels down the dendrite to the soma (the site of spike initiation). In essence, the soma receives a low-pass-filtered version of the original auditory-nerve input. Thus the temporal patterns of these inputs will only be preserved at low frequencies. This effect is in contrast to the properties of CN "bushy" cells, where auditory-nerve fibers make secure contact with the cell soma. Here, the auditory-nerve input is not subject to dendritic filtering and the temporal patterns of the inputs are preserved in the output of the cell (Oertel, 1985).

We combined the dendrite/soma model with a model of the auditory periphery. This composite model produced a number of realistic responses to pure-tone and amplitude-modulated stimuli. The model has a number of free parameters and, in such cases, it is often easy to explain one or two major qualitative results. However, as we have shown above, the model produces a large number of realistic *in vivo* response properties with a single parameter set.

One of the most important results of the model is the encoding of amplitude modulation. Although most neurons in the VCN show some enhancement of AM encoding compared to the auditory nerve, the effect has been most widely reported for stellate/chop-S cells (e.g., Frisina *et al.*, 1990a). Stellate/chop-S cell modulation transfer functions show a level dependence whereby they are low pass at low stimulus levels and bandpass at moderate and high stimulus levels.

While the exact mechanism responsible for the decrease in modulation gain at low frequencies of modulation is unknown, Frisina *et al.* (1990b) suggested that the source of the mechanism may lie in the distribution of auditory-nerve input to the dendrites of the stellate neuron. Using the model described in this article, we can show that Frisina's proposal is tenable. An examination of model outputs (Fig. 15) helps us to specify the exact mechanism. Consider AM-stimuli modulated at low frequencies (e.g., 50 Hz). At low stimulus levels [Fig. 15(a)], the mean current delivered to the cell soma is relatively low (0.1 nA) and some degree of modulation is present in the waveform applied to the cell. The stellate neuron will tend to fire [shown by dotted lines in Fig. 15(a)] at or near the peak of the each cycle in the waveform. In this case, the temporal synchronization between the original AM-stimulus and the stellate-neuron output is high and therefore the modulation gain is high. At high stimulus levels [Fig. 15(b)], again some low-frequency modulation remains in the waveform after the dendritic filtering, however, the dc bias on the signal is relatively high (mean input to soma = 0.4 nA for 50-dB input compared to 0.1 nA for 10-dB input). In this case, the neuron does not fire at the peak of each cycle, but is forced to fire as soon as its recovery period is complete. That is, it fires at its natural chopping frequency. Thus the temporal synchronization between the original input stimulus is low and therefore the modulation gain is low.

The model MTFs are very similar to the neural data. One unresolved issue, however, concerns the secondary best-modulation frequency peak present in the model MTFs which is not seen in the neural data. This issue can only be

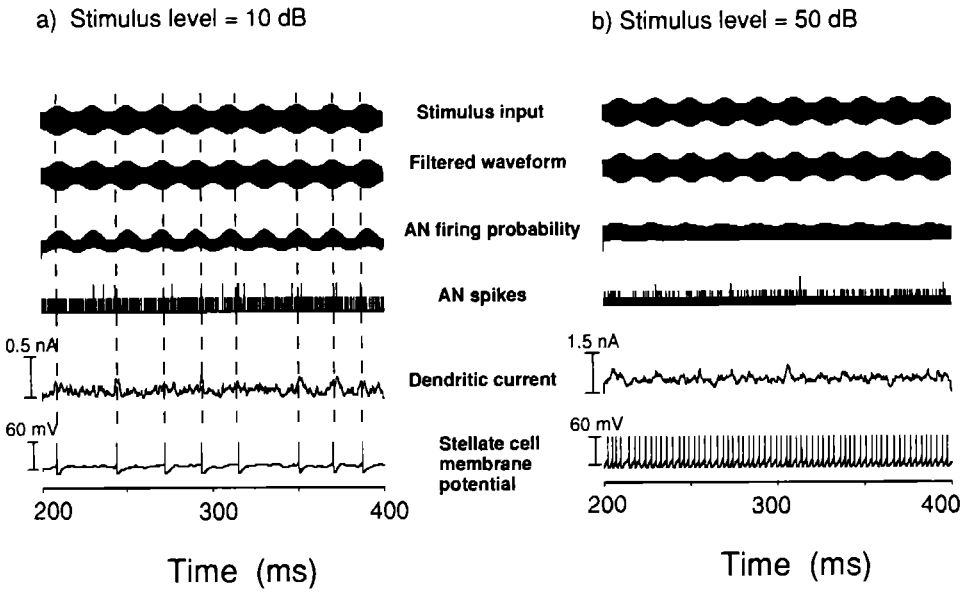

FIG. 15. Model output in response to AM-stimuli modulated at 50 Hz, carrier frequency: 5 kHz, 35% AM for two different input levels. (a) 10 dB above threshold and (b) 50 dB above threshold. The last 200 ms of a 400-ms signal are shown. The signal at the output of the filter is relatively unchanged from the input signal. This is because the sideband frequencies of the AM stimulus are within the passband of the filter and are, therefore, subject only to minimal attenuation. The AN firing probability represents the output of the Meddis hair cell model. "AN spikes" represents the instantaneous summation of all inputs to the cell. Each epoch is equal to the step integration size of the model (20 μs). In some instances, more than one spike is delivered to the cell. The input to the cell is low pass filtered to simulate dendritic processing, before being passed to the model soma.

settled with experiments using greater modulation frequency resolution.

Although the model replicates many properties of peripheral auditory responses and at the level of the cochlear nucleus stellate cells it could be developed further. For instance, we have not modeled the nonlinear basilar membrane responses (e.g., Johnstone *et al.*, 1986) or the different spontaneous-rate groups of auditory-nerve fibers (Liberman, 1978).

Another area in which the model could be developed concerns the nature of input to the stellate cell. In the model, all input to the stellate cell is excitatory. This is in contrast to the evidence provided by anatomical and physiological studies of stellate neurons which suggest that stellate cells receive both excitatory and inhibitory input. For instance, Oertel and her colleagues (1983, 1985; Oertel *et al.*, 1988) recorded both excitatory and inhibitory post-synaptic potentials in stellate cells maintained *in vitro* in response to auditory-nerve stimulation. Anatomical studies have noted that input to stellate cells is both cochlear and noncochlear in origin (e.g., Brawer and Morest, 1975). However, these studies did not determine whether they were studying type-I or type-II stellate cells. It is possible, therefore, that the type-I (chop-S) units receive only excitatory input as suggested by Blackburn and Sachs (1989).

Another aspect of the current model is that accurate model responses were generated using a relatively simple low-pass filter to simulate dendritic filtering. Young *et al.* (1988b) have previously suggested that the effects of dendritic filtering were far more severe than could be expected from a first-order filter of the type used here. However, recent evidence from Smith and Rhode (1989) has shown that the majority of AN inputs to type-I stellate cells synapse very close (within 100 μm) of the soma. Models of dendrites based on cable theory predict that dendritic inputs close to the soma are subject to only limited low-pass filtering compared to those that synapse at more distal points on the dendrite. In this study, we have approximated these effects with a simple low-pass filter. One limitation of this approach, however, is that we cannot explicitly incorporate the data of Smith and Rhode (1989) into the model. More detailed modeling of dendritic filtering are reported in Banks and Sachs (1991).

In this paper, we have successfully modeled the temporal encoding of amplitude modulation by cochlear-nucleus stellate neurons. The processing of amplitude modulation by these neurons has given rise to the suggestion that these neurons are "feature detectors." However, in themselves, these neurons do not directly help us to identify the rate of modulation in a given channel. They merely amplify the temporal encoding of complex sound features such as amplitude modulation. Above a relatively low signal level, the output spike rate is the same for all AM rates; it is only the pattern of timing of the spikes which changes. To identify the actual AM rate we need another stage. It is possible that neurons in the central nucleus of the inferior colliculus (ICC) could provide the necessary transformation to convert the temporal information into a place representation. Certain neurons in the ICC have been shown to be tuned to particular rates of amplitude modulation (Rees and Møller, 1987; Langner and Schreiner, 1988; Rees and Palmer, 1988). However, they also show an increase in firing rate with an increase in the depth of AM. The cells are organized topographically and suggest that AM is coded by a rate-place system in the ICC. We are currently studying the effects of simple coincidence detector cells fed from a number of model stellate cells. Preliminary modeling work in our laboratory has shown that such cells can recode temporal AM information into a rate-place representation.

V. CONCLUSIONS

We have presented and evaluated a computer model of a ventral-cochlear-nucleus stellate cell with chop-S type responses. The structure of the model was constrained by the known anatomy of stellate cells. The basic membrane prop-

erties of the cell were modeled according to data from the *in vitro* work of Oertel. When driven by auditory-nerve spikes generated by a simulation of the auditory periphery, the basic dendrite/soma unit was able to generate a large number of realistic response properties to AM and pure-tone stimuli.

ACKNOWLEDGMENTS

This work was supported by a SERC research Image Interpretation Initiative grant. We are indebted to Ian Winter and the two anonymous reviewers who read and commented on the first draft of this paper.

[1] It is important to note that the enhancement of modulation is achieved by the stellate cells, and is not due to processing at a peripheral site such as auditory-nerve fibers. Physiological studies have demonstrated that auditory-nerve fiber modulation transfer functions are broad lowpass functions at low stimulus levels and irregular and broad irregular functions with low-modulation gains at high stimulus levels (Møller, 1976; Javel, 1980; Frisina, 1983; Frisina *et al.*, 1990a). The same features were observed in the modulation transfer functions of the hair-cell simulation used in the composite model.

Adams, J. C. (1979), "Ascending projections to the inferior colliculus," J. Comp. Neurol. **183**, 519–538.

Arle, J. E., and Kim, D. O. (1991). "Neural modeling of intrinsic and spike-discharge properties of cochlear nucleus neurons," Biol. Cyber. **64**, 273–283.

Banks, M. I., and Sachs, M. B. (1991). "Regularity analysis in a compartmental model of chopper units in the anteroventral cochlear nucleus," J. Neurophysiol. **65**, 606–629.

Beauchamp, K. G., and Yuen, C. K. (1979). *Digital Methods for Signal Analysis* (Allen and Unwin, London).

Blackburn, C. C., and Sachs, M. B. (1989). "Classification of unit types in the anteroventral cochlear nucleus: PST histograms and regularity analysis," J. Neurophysiol. **62**, 1303–1329.

Blackburn, C. C., and Sachs, M. B. (1990). "The representation of the steady-state vowel sound /ɛ/ in the discharge patterns of cat anteroventral cochlear nucleus neurons," J. Neurophysiol. **63**, 1191–1212.

Bourk, T. R. (1976). "Electrical responses of neural units in the anteroventral cochlear nucleus of the cat," Ph.D. thesis, Massachusetts Institute of Technology, Cambridge, MA.

Brawer, R. J., Morest, D. K., and Kane, E. C. (1974). "The neuronal architecture of the cochlear nucleus of the cat," J. Comp. Neurol. **155**, 251–300.

Brawer, R. J., and Morest, D. K. (1975). "Relation between auditory nerve endings and cell types in the cat's anteroventral cochlear nucleus seen with the Golgi method and Normarski optics," J. Comp. Neurol. **160**, 491–506.

Cant, N. B. (1981). "The fine structure of two types of stellate cells in the anterior division of the anteroventral cochlear nucleus of the cat," Neuroscience **6**, 2643–2655.

Cant, N. B. (1982). "Identification of cell types in the anteroventral cochlear nucleus that project to the inferior colliculus," Neurosci. Lett. **32**, 241–246.

Cant, N. B., and Morest, D. K. (1984). "The structural basis for stimulus coding in the cochlear nucleus of the cat," in *Hearing Science, Recent Advances*, edited by C. I. Berlin (College Hill, San Diego), pp. 371–421.

Frisina, R. D. (1983). "Enhancement of responses to amplitude modulation in the gerbil cochlear nucleus: Single-unit recordings using an improved surgical approach," Dissertation and Special Report ISR-S-23, Institute for Sensory Research, Syracuse, NY.

Frisina, R. D., Smith, R. L., and Chamberlin, S. C. (1985). "Differential encoding of rapid changes in sound amplitude by second-order auditory neurons," Exp. Brain Res. **60**, 417–422.

Frisina, R. D., Smith, R. L., and Chamberlin, S. C. (1990a). "Encoding of amplitude modulation in the gerbil cochlear nucleus: I. A hierarchy of enhancement," Hear. Res. **44**, 99–122.

Frisina, R. D., Smith, R. L., and Chamberlin, S. C. (1990b). "Encoding of amplitude modulation in the gerbil cochlear nucleus: II. Possible neural mechanisms," Hear. Res. **44**, 123–142.

Ghoshal, S., Kim, D. O., and Northrop, R. B. (1990). "A modeling study of amplitude-modulated tone encoding behavior of cochlear nucleus neurons," Soc. Neurosci. Abstr. **16**, 871.

Godfrey, D. A., Kiang, N. Y. S., and Norris, B. E. (1975), "Single unit activity in the posteroventral cochlear nucleus of the cat," J. Comp. Neurol. **162**, 247–268.

Goldberg, J. M., and Brown, P. B. (1969). "Responses of binaural neurons of dog superior olivary complex to dichotic tonal stimulation: Some physiological mechanisms of sound localization," J. Neurophysiol. **32**, 940–958.

Hackney, C. M., Osen, K. K., and Kolston, J. (1990). "Anatomy of the cochlear nuclear complex of guinea pig," Anat. Embryol. **182**, 123–149.

Hastings, N. A. J., and Peacock, J. B. (1975). Statistical distributions (Butterworths, London).

Hewitt, M. J., and Meddis, R. (1991). "An evaluation of eight computer models of mammalian inner hair-cell function," J. Acoust. Soc. Am. **90**, 904–917.

Javel, E. (1980). "Coding of AM tones in the chinchilla auditory nerve: Implications for the pitch of complex tones," J. Acoust. Soc. Am. **68**, 133–146.

Johnson, D. H. (1980). "The relationship between spike rate and synchrony in responses of auditory-nerve fibers to single tones," J. Acoust. Soc. Am. **68**, 1115–1122.

Johnstone, B. M., Patuzzi, R., and Yates, G. K. (1986). "Basilar membrane measurements and the traveling wave," Hear. Res. **22**, 147–153.

Kim, D. O., Sirianni, J. G., and Chang, S. O. (1990). "Responses of DCN-PVCN neurons and auditory nerve fibers in unanesthetized decerebrate cats to AM and pure tones: Analysis with autocorrelation/power-spectrum," Hear. Res. **45**, 95–113.

Langner, G., and Schreiner, C. E. (1988). "Periodicity coding in the inferior colliculus of the cat: I. Neuronal mechanisms," J. Neurophysiol. **60**, 1799–1822.

Liberman, M. C. (1978). "Auditory-nerve responses from cats raised in a low-noise chamber," J. Acoust. Soc. Am. **63**, 442–455.

MacGregor, R. J. (1987). *Neural and Brain Modeling* (Academic, San Diego).

Meddis, R. (1986). "Simulation of mechanical to neural transduction in the auditory receptor," J. Acoust. Soc. Am. **79**, 702–711.

Meddis, R. (1988). "Simulation of auditory-neural transduction: Further studies," J. Acoust. Soc. Am. **83**, 1056–1063.

Meddis, R., (1990). "A physiological model of auditory selective attention," in *Cochlear Nucleus: Structure and Function in Relation to Modeling*, edited by W. A. Ainsworth (JAI, Ltd., London) (in press).

Meddis, R., and Hewitt, M. J. (1991). "Virtual pitch and phase sensitivity of a computer model of the auditory periphery: I. Pitch identification," J. Acoust. Soc. Am. **89**, 2866–2882.

Meddis, R., Hewitt, M. J., and Shackleton, T. M. (1990). "Implementation details of a computational model of the inner hair-cell/auditory-nerve synapse," J. Acoust. Soc. Am. **87**, 1813–1818.

Møller, A. R. (1972). "Coding of amplitude and frequency modulated sounds in the cochlear nucleus of the rat," Acta Physiol. Scand. **86**, 223–238.

Møller, A. R. (1973). "Statistical evaluation of the dynamic properties of cochlear nucleus units using stimuli modulated with pseudo-random noise," Brain Res. **57**, 443–456.

Møller, A. R. (1974). "Responses of units in the cochlear nucleus to sinusoidally amplitude-modulated tones," Exp. Neurol. **45**, 104–117.

Møller, A. R. (1976). "Dynamic properties of primary auditory fibers compared with cells in the cochlear nucleus," Acta Physiol. Scand. **98**, 157–167.

Oertel, D. (1983). "Synaptic responses and electrical properties of cells in brain slices of the mouse anteroventral cochlear nucleus," J. Neurosci. **3**, 2043–2053.

Oertel, D. (1985). "Use of brain slices in the study of the auditory system: spatial and temporal summation of synaptic inputs in cells in the anteroventral cochlear nucleus of the mouse," J. Acoust. Soc. Am. **78**, 328–333.

Oertel, D., Wu, S. H., and Hirsch, J. A. (1988). "Electrical characteristics of cells and neuronal circuitry in the cochlear nuclei studied with intracellular recordings from brain slices," in *Auditory Function*, edited by G. M. Edelman, W. E. Gall, and W. M. Cowan (Wiley, New York), pp. 313–336.

Osen, K. K. (1969). "Cytoarchitecture of the cochlear nuclei in the cat," J.

Comp. Neurol. **136**, 453–483.
Osen, K. K. (**1972**). "Projection of the cochlear nuclei on the inferior colliculus in cat," J. Comp. Neurol. **144**, 355–372.
Patterson, R. D., Nimmo-Smith, I., Holdsworth, J., and Rice, P. (**1988**). "Spiral Vos final report, Part A: The auditory filterbank," Cambridge Electronic Design, Contract Rpt. APU, 2341.
Pfeiffer, R. R. (**1966**). "Classification of response pattern of spike discharges for units in the cochlear nucleus: Tone burst stimulation," Exp. Brain Res. **1**, 220–235.
Rall, W. (**1989**). "Cable theory for dendritic neurons," in *Methods in Neuronal Modeling: From Synapses to Networks*, edited by C. Koch and I. Segev (MIT, Cambridge, MA), pp. 9–62.
Rees, A., and Møller, A. R. (**1987**). "Stimulus properties influencing the responses of inferior colliculus neurons to amplitude-modulated sounds," Hear. Res. **27**, 129–143.
Rees, A., and Palmer, A. R. (**1988**). "Rate-intensity functions and their modification by broadband noise for neurons in the guinea-pig inferior colliculus," J. Acoust. Soc. Am. **83**, 1488–1499.
Rhode, W. S., Oertel, D., and Smith, P. H. (**1983**). "Physiological response properties of cells labeled intracellularly with horseradish perioxidase in the cat ventral cochlear nucleus," J. Comp. Neurol. **213**, 448–463.
Rhode, W. S., and Smith, P. H. (**1986**). "Encoding timing and intensity in the ventral cochlear nucleus of the cat," J. Neurophysiol. **56**, 261–286.
Rose, J. E., Galambos, R., and Hughes, J. R. (**1960**). "Organization of frequency selective neurons in the cochlear nucleus complex of the cat," in *Neural Mechanisms of the Auditory and Vestibular Systems*, edited by G. L. Rasmussen and W. F. Windle (Thomas, Springfield), pp. 116–136.
Rose, J. E., Brugge, J. F., Anderson, D. J., and Hind, J. E. (**1967**). "Phase-locking responses to low-frequency tones in single auditory-nerve fibers of the squirrel monkey," J. Neurophysiol. **30**, 769–793.
Rouiller, E. M., and Ryugo, D. K. (**1984**). "Intracellular marking of physiologically characterized cells in the ventral cochlear nucleus of the cat," J. Comp. Neurol. **225**, 167–186.
Schreiner, C. E., and Langner, G. (**1988**). "Periodicity coding in the inferior colliculus of the cat: II. Topographical organization," J. Neurophysiol. **60**, 1823–1840.
Smith, P. H., and Rhode, W. S. (**1989**). "Structural and functional properties distinguish two types of multipolar cells in the ventral cochlear nucleus," J. Comp. Neurol. **282**, 595–616.
Warr, W. B. (**1982**). "Parallel ascending pathways from the cochlear nucleus: Neuroanatomical evidence of functional specialization," Contrib. Sensory Physiol. **7**, 1–38.
Winter, I. M., and Palmer, A. R. (**1990**). "Responses of single units in the anteroventral cochlear nucleus of the guinea pig," Hear. Res. **44**, 161–178.
Young, E. D., Robert, J-M., and Shofner, W. P. (**1988a**). "Regularity and latency of units in the ventral cochlear nucleus: Implications for unit classification and generation of response properties," J. Neurophysiol. **60**, 1–29.
Young, E. D., Shofner, W. P., White, J. A., Robert, J-M., and Voigt, H. F. (**1988b**). "Response properties of cochlear nucleus neurones in relationship to physiological mechanisms," in *Auditory Function*, edited by G. M. Edelman, W. E. Gall, and W. M. Cowan (Wiley, New York), pp. 277–312.